

## YAMATO-793605: A NEW LHERZOLITIC SHERGOTTITE FROM THE JAPANESE ANTARCTIC METEORITE COLLECTION

Takashi MIKOUCHI and Masamichi MIYAMOTO

*Mineralogical Institute, Graduate School of Science,  
University of Tokyo, Hongo, Bunkyo-ku, Tokyo 113*

**Abstract:** Y-793605 is a new martian meteorite from Antarctica that can be classified as a lherzolitic shergottite. Y-793605 mainly shows a poikilitic texture (large pyroxene oikocryst with enclosed olivine and chromite), but partly contains non-poikilitic areas (mainly maskelynite, olivine, and pigeonite). Olivine in the non-poikilitic area is more Fe-rich and shows a narrower compositional distribution than that in the poikilitic area. Low-Ca pyroxenes in the non-poikilitic area are also more Fe-rich ( $\text{En}_{65}\text{Fs}_{28}\text{Wo}_7 \sim \text{En}_{60}\text{Fs}_{27}\text{Wo}_{13}$ ) than those in the poikilitic area ( $\text{En}_{76}\text{Fs}_{21}\text{Wo}_3 \sim \text{En}_{66}\text{Fs}_{23}\text{Wo}_{11}$ ). Augites in the poikilitic area are usually present rimming the oikocrysts ( $\text{En}_{52}\text{Fs}_{16}\text{Wo}_{32}$  to  $\text{En}_{49}\text{Fs}_{14}\text{Wo}_{37}$ ). The crystallization sequence of minerals in Y-793605 is considered to have begun by initial crystallization of cumulus phases (olivine and chromite) from the parent magma. Then, low-Ca pyroxenes and later augite poikilitically enclosed cumulus phases, and became a large oikocryst. Due to accumulation of phases, small interstitial melts formed between the oikocryst boundaries, and plagioclase crystallized from the Ca-Fe-rich melt along with pigeonite. After minor augite crystallization in the non-poikilitic area, all phases experienced re-equilibration (*e.g.*, homogenization of olivine). Y-793605 shows a close relationship to previously known lherzolitic shergottites ALH77005 and LEW88516. Especially, olivine composition of Y-793605 is nearly identical to that of LEW88516. Pyroxene and maskelynite compositions are almost the same among these three meteorites. Although it is hardly possible to consider that Y-793605 is paired with ALH77005 or LEW88516 in the sense that Y-793605 was in the same fall with them, it can be concluded that Y-793605 originated from the same igneous body or rock in Mars as ALH77005 and LEW88516.

### 1. Introduction

SNC (shergottites, nakhlites and chassignite) meteorites are widely believed to have originated from the planet Mars, and they have offered valuable information on martian igneous processes because they all are igneous rocks (*e.g.*, MCSWEEN, 1985, 1994). Totally 12 martian meteorites have been known up to date, and 6 of them have been recovered by Japanese and American expedition to Antarctica. SNC meteorites show a wide range of petrologically different characteristics, and they are considered to represent geologically different origin of the rocks. One of the SNC meteorite (ALH84001 orthopyroxenite) contains ~1 vol% carbonates (TREIMAN, 1995) and was recently reported to bear the possibility that a primitive form of microscopic life may have existed on Mars more than three billion years ago (MCKAY *et al.*, 1996). Thus, SNC meteorites even have possibilities to give us extraterrestrial biological informa-

tion.

Shergottite is the largest group of SNC meteorites, and it can be divided into two sub-groups, basaltic shergottites and lherzolitic shergottites (*e.g.*, MCSWEEN, 1994). The 16 g small meteorite Yamato-793605 (Y-793605) in the Japanese Antarctic meteorite collection was recently described as a new member of SNC meteorites (MAYEDA *et al.*, 1995; YANAI, 1995). Y-793605 shows a close relationship to previously known lherzolitic shergottites (MIKOUCHI and MIYAMOTO, 1996a, b). ALH77005 and LEW88516 have been the only known lherzolitic shergottites that show similar mineralogical and petrological characteristics to each other, and they are considered to share the same original source in Mars (HARVEY *et al.*, 1993; TREIMAN *et al.*, 1994). The name of ALHA77005 is used in Antarctic Meteorite Newsletter, while ALH-77005 is used in Catalog of Japanese Collection of the Antarctic Meteorites, because this meteorite was separated in half between Japan and USA. In this paper, we call the meteorite "ALH77005". Lherzolitic shergottites are characterized by the presence of poikilitic texture of the rocks. Large oikocrysts of pyroxene enclose cumulus Mg-rich olivine and chromite. Lherzolitic shergottites also contain a volumetrically minor non-poikilitic texture. These rocks possibly crystallized from a melt parental to those from which basaltic shergottites had crystallized or they are peridotite type samples from which parent magmas of basaltic shergottites were derived by partial melting (MCSWEEN *et al.*, 1979a, b). Discovery of Y-793605 has a potential to give us another important aspect on petrology of lherzolitic shergottites.

In this paper, we report mineralogical and petrological data of Y-793605 as a part of the consortium investigation of this small martian meteorite organized by National Institute of Polar Research (NIPR) to understand the petrogenesis of this rock, and discuss its petrogenetic relationship to the other lherzolitic shergottites ALH77005 and LEW88516.

## 2. Sample and Analytical Techniques

A polished thin section (PTS) of Y-793605 (Y-793605,51-2) was generously supplied by NIPR. Petrographic observations and chemical analyses were made on the PTS by optical and electron microscopy. The electron microscopy was performed in the Electron Microbeam Analysis Facility of the Mineralogical Institute, University of Tokyo. Several single pyroxene grains (~1 mm in size) were also supplied, and they were analyzed by a single crystal X-ray diffraction technique (precession method). Backscattered electron images were taken with a JEOL JXA840 scanning electron microscope with an energy dispersive spectrometer (EDS). Quantitative wavelength dispersive analyses were performed on a JEOL 733 electron microprobe (Ocean Research Institute, University of Tokyo) and a JEOL JCM 733 mk II microprobe (Geological Institute, University of Tokyo). Microprobes were operated at 15 kV accelerating voltage, and beam current was 12 nA on Faraday cages. In analysis of some maskelynites and glasses, a broad beam about 10  $\mu\text{m}$  in diameter was employed to minimize loss of volatile elements. Elemental distribution maps were obtained by a JEOL JXA 8900L electron microprobe (Geological Institute, University of Tokyo). Accelerating voltage was 15 kV and beam current was 120 nA on Faraday cage. We

counted the element intensity at peak wavelength for 30 ms for each pixel of the measured area.

### 3. Results

#### 3.1. Petrography

Y-793605,51-2 is about  $9 \times 6$  mm in size. It principally shows a typical poikilitic texture, but partly contains a non-poikilitic, interstitial area (Fig. 1). The boundary between the poikilitic and non-poikilitic area is continuous, but not straight. The non-poikilitic area distributes as a narrow winding band up to 1–2 mm in width (Figs. 1, 2). A shock-induced melt vein which is about  $100 \mu\text{m}$  wide is cutting the PTS. The vein is composed of very fine-grained material with lithic fragments of olivine, pyroxenes, and chromite (Fig. 3). Y-793605 is composed of olivine, low-Ca pyroxenes, augite, maskelynite, chromite, and a few other accessory minerals. No Ca-phosphate grain has been identified throughout the PTS. The modal abundances of minerals in Y-793605,51-2 except an impact melt vein are 40% olivine, 33% low-Ca pyroxenes, 17% augite, 8% maskelynite, 1.5% opaque phases (Cr-rich spinels and ilmenite), and 0.5% others (mainly glass).

In the poikilitic area, a large pyroxene oikocryst that is larger than 8 mm across encloses rounded olivines and aggregates of chromite (Fig. 4). The pigeonite area of the oikocryst has coarse twin bands ( $\sim 1.5$  mm in width) that are partially faulted probably due to intense shock (Fig. 5). Undulatory extinction and two-sets of linear structure of the pyroxene oikocryst are observed under an optical microscope (Fig. 6), and they would be also produced by a shock effect. The oikocryst contains augites usually along its edge (Fig. 7). They are irregular in shape, and they do not follow the specific crystallographic orientations. Augites are also present as irregular patches within the oikocryst. Olivines in the oikocryst are brownish green in color and their sizes reach up to 1.5 mm in longer dimension. Most olivines are round in shape, and are extensively altered along their rims and interior fractures (Fig. 4). The altered portions are turned into dark brown in color probably due to presence of  $\text{Fe}^{3+}$  during shock oxidation on Mars (HARVEY *et al.*, 1993). Olivine also exhibits undulatory extinction. Chromites in the oikocryst are euhedral (square-shaped) in texture ( $\leq 100 \mu\text{m}$ ) and they are scattered in the oikocryst. Usually they are present as aggregates of several grains (Fig. 8). Maskelynites are rarely observed in the poikilitic area, but small maskelynite grains (up to a few hundreds  $\mu\text{m}$  across) are present, usually in or near the augite patches. Some subrounded magmatic inclusions are contained near the centers of the olivine crystals (Fig. 9). They are usually  $\sim 100 \mu\text{m}$  in size, but the largest inclusion reaches  $400 \mu\text{m}$  in size (Fig. 9b). The inclusion consists of several unique phases such as Al-Ti-rich pyroxene (both low and high-Ca pyroxenes) and Si-rich feldspathic glass. Typically, pyroxenes are present as elongated crystals in the host of Si-rich glass (Fig. 9a). Some pyroxenes are nucleating on the surrounding olivine walls. The pyroxenes in the largest inclusion do not show elongated textures (Fig. 9b).

The non-poikilitic area is formed by almost the same sizes ( $\sim 1$  mm across) of olivine, maskelynite and pyroxenes (Fig. 10). Olivine and maskelynite are more abundant than pyroxenes in the non-poikilitic area. Olivines in the non-poikilitic area are

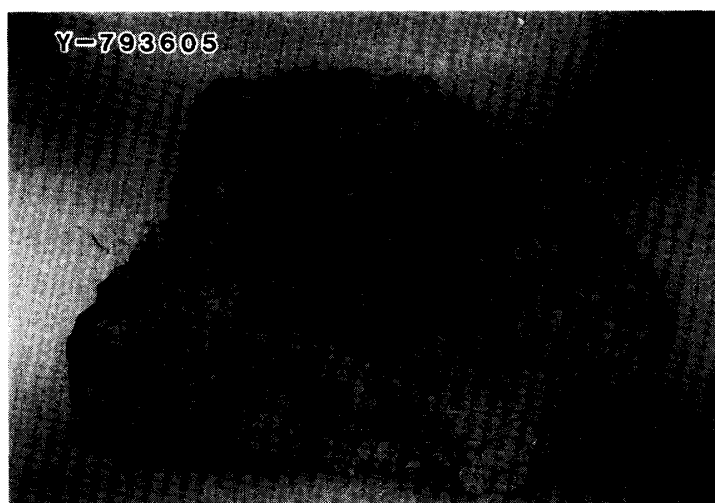


Fig. 1a. Photomicrograph of Y-793605,51-2. Transmitted plain polarized light. The width of field is approximately 10 mm.



Fig. 1b. Backscattered electron (BSE) image of Y-793605,51-2. A large pyroxene oikocryst is present (dark gray), and it is zoned from darker grayish part (left bottom) to brighter part (right bottom ~ center top). Olivine (bright gray) and chromite (small white grains) are enclosed by the oikocryst. Non-poikilitic area is also present (right top), and it is composed of maskelynite (black), olivine (bright gray), and pigeonite (dark gray).

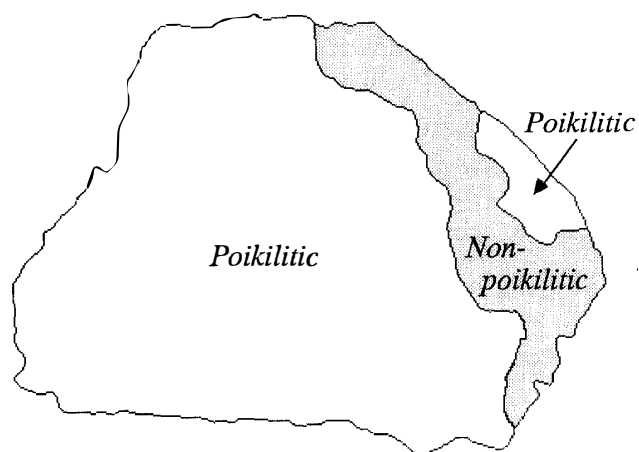


Fig. 1c. Schematic illustration showing the boundary between the poikilitic and non-poikilitic areas.

Fig. 2a. BSE image of the boundary between the poikilitic and non-poikilitic areas of Y-793605, 51-2. The non-poikilitic area including abundant maskelynite is distinct from the poikilitic area. Note that maskelynites crystallized from the wall of the poikilitic area. Px: pyroxenes, Ol: olivine, Ms: maskelynite, and Cr: chromite. Scale bar is 1 mm.

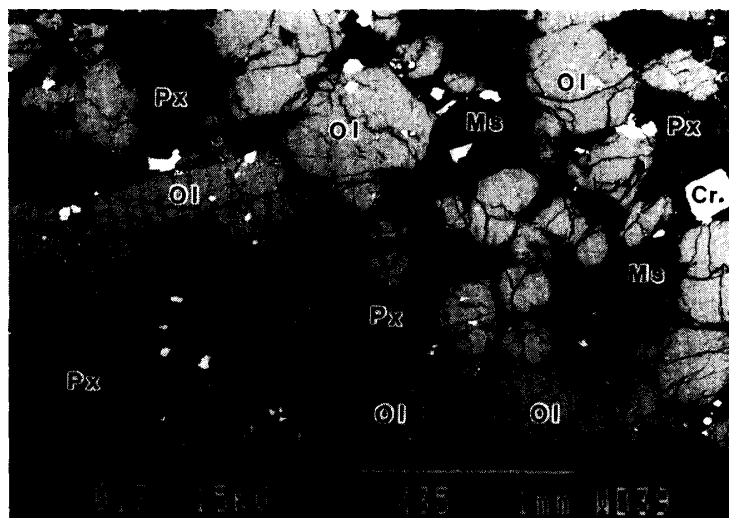


Fig. 2b. Schematic illustration showing the boundary between poikilitic and non-poikilitic areas.

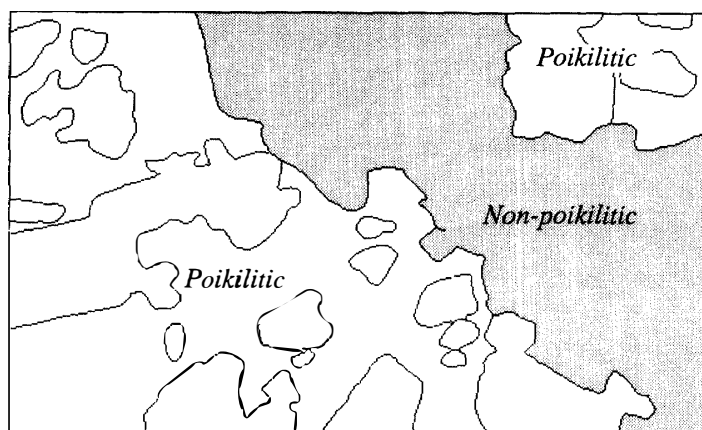
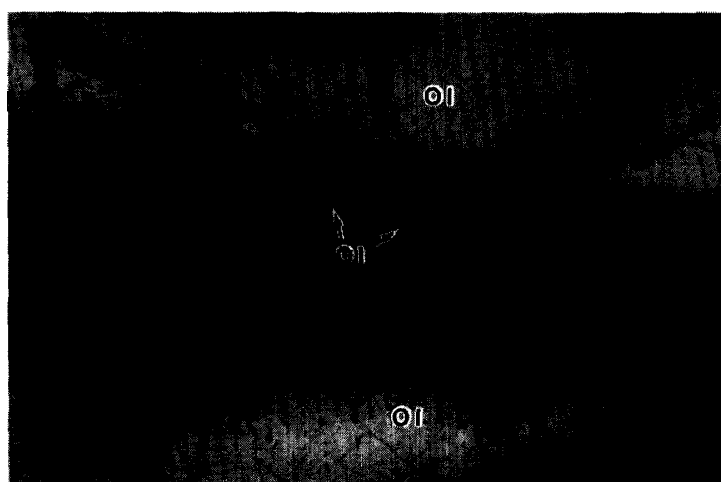


Fig. 3. Photomicrograph of the impact melt vein in Y-793605, 51-2. Transmitted plain polarized light. The vein is cutting the olivine single crystal. The vein is composed of very fine-grained materials. Larger lithic fragments of the surrounding minerals (olivine, pyroxenes, and chromite) are also present. Ol: olivine. The width of field is approximately 0.65 mm.



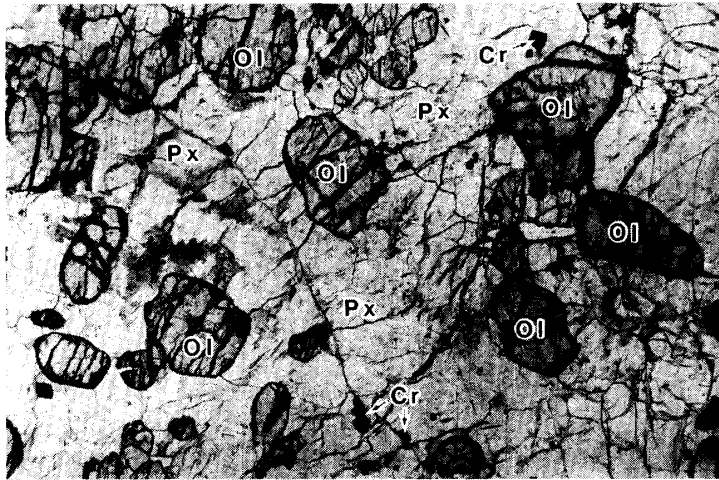


Fig. 4a. Photomicrograph of the typical poikilitic area in Y-793605,51-2. Transmitted plain polarized light. Rounded olivines and chromite aggregates are present in the oikocryst. Ol: olivine, Px: pyroxenes, and Cr: chromite. The width of field is approximately 3.2 mm.

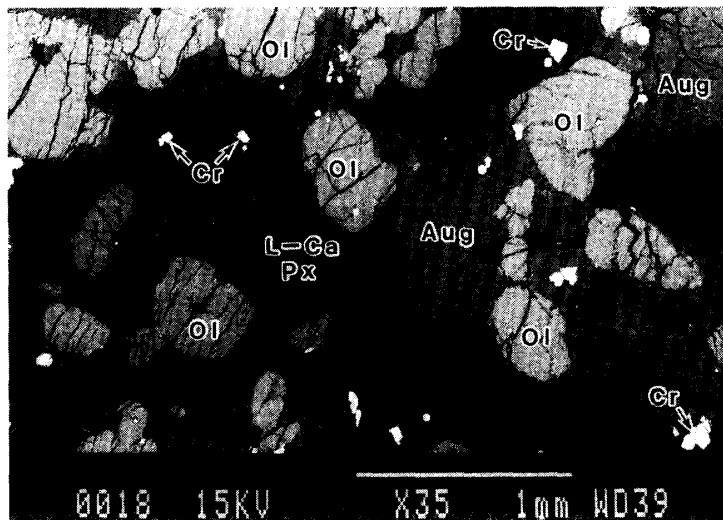


Fig. 4b. BSE image of the typical poikilitic area. Almost same area as shown in Fig. 4a. The pyroxene oikocryst has patches of augite (brighter gray than the host). Ol: olivine, L-Ca Px: low-Ca pyroxene, Aug: augite, and Cr: chromite.

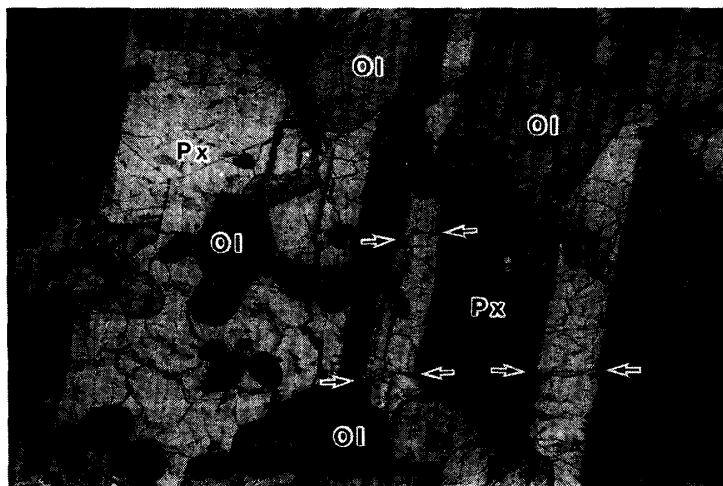


Fig. 5. Photomicrograph of the pyroxene oikocryst in Y-793605,51-2. Crossed polarized light. Coarse twin bands are present, and they are partly faulted by intense shock (arrows). Ol: olivine and Px: pyroxenes. The width of field is approximately 3.2 mm.

Fig. 6. Photomicrograph of the pyroxene oikocryst in Y-793605, 51-2. Crossed polarized light. It is obvious that the pyroxene has a streak texture that is parallel to two directions. Ol: olivine and Px: pyroxenes. The width of field is approximately 0.65 mm.

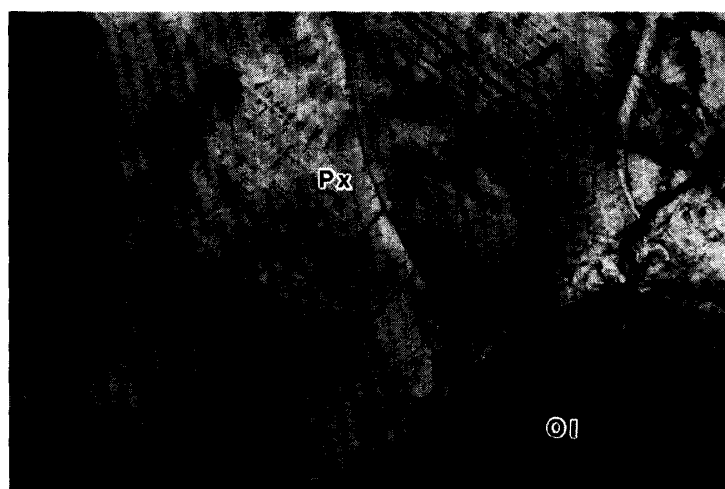


Fig. 7. Ca elemental image of the pyroxene oikocryst in Y-793605, 51-2. Brighter areas correspond to higher Ca concentration. In this image, olivines are black, while augites are white. Note that augite is present along the rims of the oikocryst as well as the interior patches. Top right is the non-poikilitic area. Ol: olivine, L-Ca Px: low-Ca pyroxene, Aug: augite, and Ms: maskelynite.

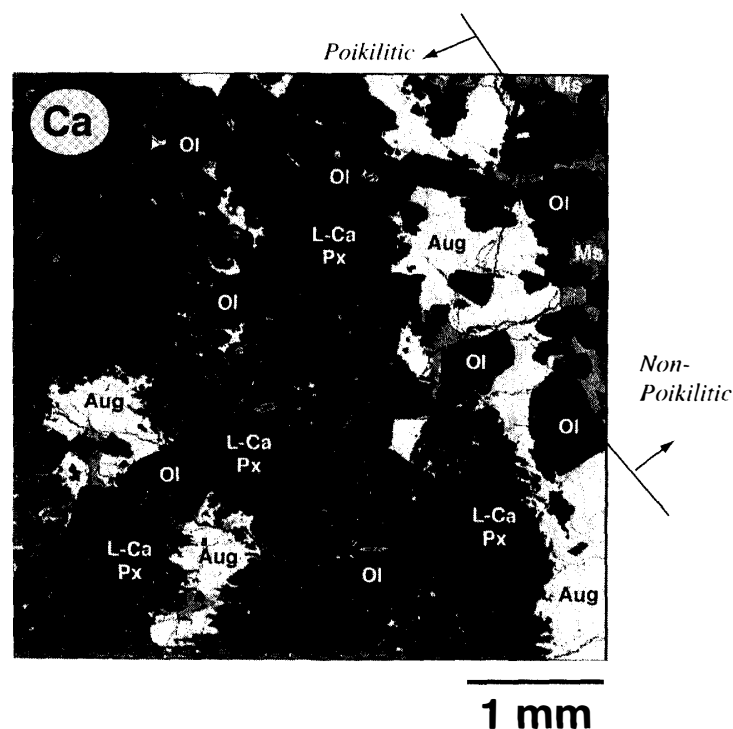
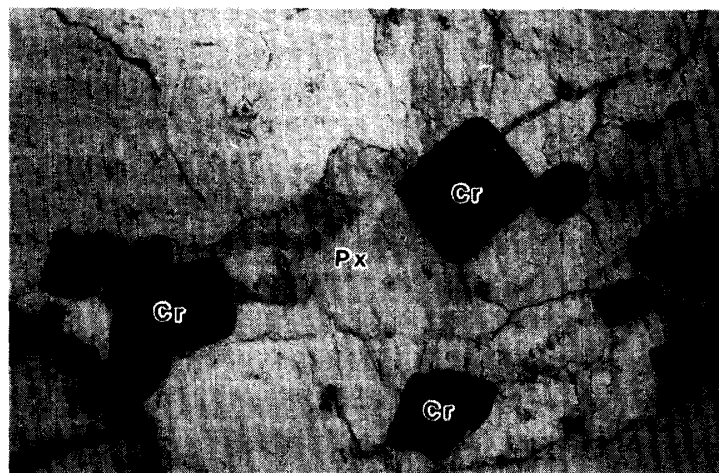


Fig. 8. Photomicrograph of the chromite aggregates in the pyroxene oikocryst of Y-793605, 51-2. Transmitted plain polarized light. Chromites in the oikocryst are generally ~100  $\mu\text{m}$  in size. Cr: chromite and Px: pyroxenes. The width of field is approximately 0.65 mm.



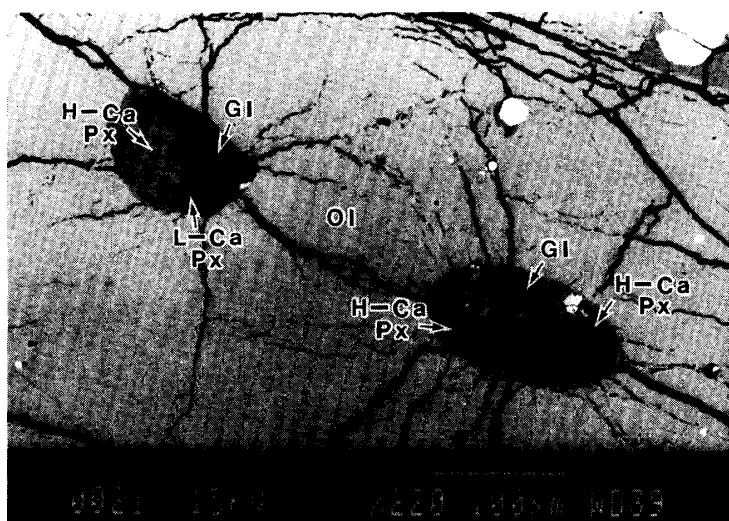


Fig. 9a. BSE image of two trapped magmatic inclusions in olivine of Y-793605,51-2. The left inclusion is composed of Si-rich glass and pyroxenes. The pyroxene contains both Ca-rich and Ca-poor compositions. The right inclusion is also composed of Si-rich glass and pyroxenes, but texturally different from that in the left. Elongated crystals are pyroxenes, and they are mainly high-Ca pyroxene. Pyroxenes are also surrounding the wall of the enclosing olivine. Gl: Si-rich glass, Ol: olivine, L-Ca Px: low-Ca pyroxene, H-Ca Px: high-Ca pyroxene. Scale bar is 0.1 mm.

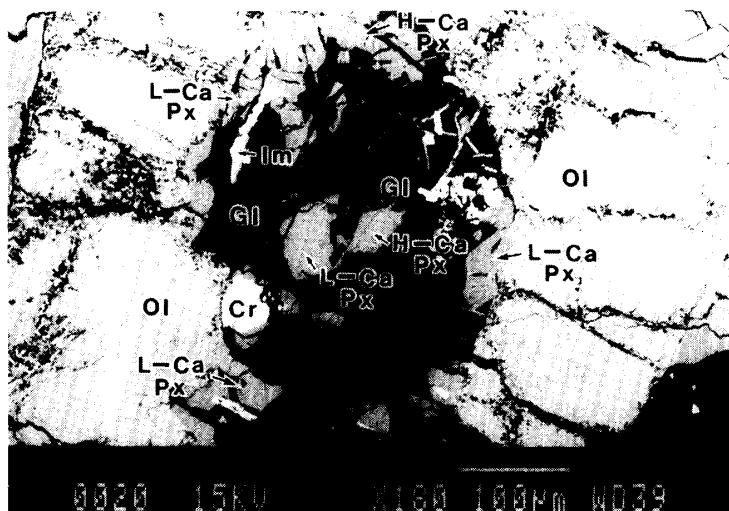


Fig. 9b. BSE image of the largest trapped magmatic inclusion in olivine of Y-793605,51-2. Two kinds of Si-rich glasses are dominated in the inclusion. Al-Ti-rich pyroxenes of both Ca-poor and Ca-rich compositions are present. Ilmenite in the inclusion is elongated. The black-colored areas in the glass are rich in Si. Gl: Si-rich glass, Ol: olivine, L-Ca Px: low-Ca pyroxene, H-Ca Px: high-Ca pyroxene, Im: ilmenite, and Cr: chromite. Scale bar is 0.1 mm.

somewhat angular in shape unlike those in the poikilitic area, but their sizes are generally similar in both textures (Fig. 1). Maskelynites in the non-poikilitic area is elongated in shape, and their longer dimensions are usually perpendicular to the direction of the non-poikilitic band (Fig. 10). Maskelynite in the non-poikilitic area sometimes contains inclusions of pyroxene and several other phases. Unlike the poikilitic area, almost all pyroxenes are pigeonite. Pigeonite is colorless and usually has two well developed sets of cleavage. Augite is rarely observed, probably due to a small volume fraction of pyroxenes in the non-poikilitic area. An Fe-P-rich phase is also included in the non-poikilitic area (Fig. 11).

Although MAYEDA *et al.* (1995) and YANAI (1995) previously reported that Y-793605 is brecciated, our PTS does not show such a texture. This shows a local sample heterogeneity of this meteorite.

### 3.2. Mineral compositions

Representative chemical compositions of several major and minor phases in Y-793605 are listed in Tables 1 and 2.

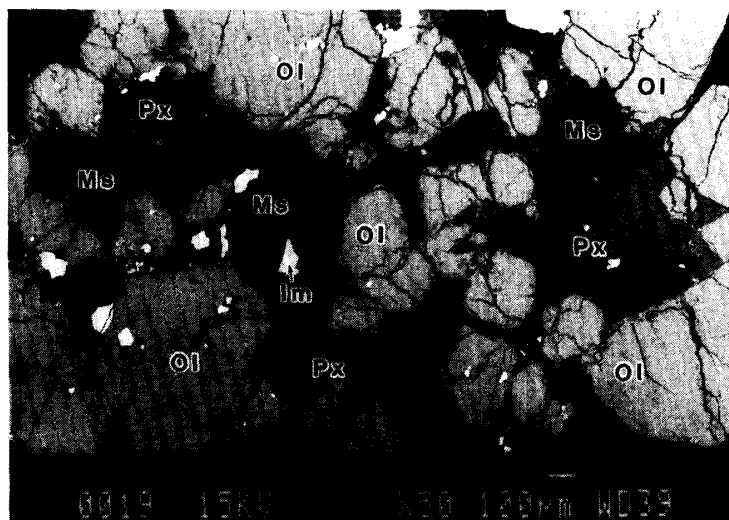


Fig. 10. BSE image of the non-poikilitic area of Y-793605,51-2. Maskelynites are much more abundant than in the poikilitic area. Px: pyroxenes, Ol: olivine, Ms: maskelynite, and Im: ilmenite. Scale bar is 0.1 mm.

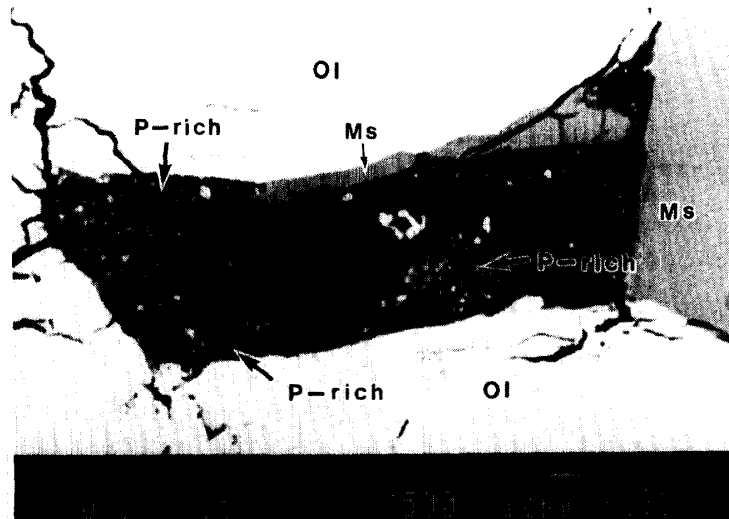


Fig. 11. BSE image of the P-rich phase in the non-poikilitic area. P-rich phases are very fine-grained, and their real compositions are unclear. Dark areas near the center are voids. P-rich: P-rich phase, Ol: olivine, and Ms: maskelynite. The photo is overexposed to obtain the bright image of P-rich phases. Scale bar is 10  $\mu\text{m}$ .

### 3.2.1. Pyroxenes

The pyroxene oikocryst is chemically zoned from a Ca-poor composition ( $\text{En}_{76}\text{Fs}_{21}\text{Wo}_3$ ) to a relatively Ca-Fe-rich composition ( $\text{En}_{66}\text{Fs}_{23}\text{Wo}_{11}$ ) (Fig. 12). The zoning is continuous and there is little scattering in Fe content. The lowest-Ca pyroxene ( $\text{Wo}_3$ ) has chemically an orthopyroxene composition, but its structural state is unclear. Augite in the poikilitic area is also zoned usually from  $\text{En}_{52}\text{Fs}_{16}\text{Wo}_{32}$  to  $\text{En}_{49}\text{Fs}_{14}\text{Wo}_{37}$  (Fig. 12). The equilibration temperature using a two pyroxene thermometer (LINDSLEY and ANDERSEN, 1983) gives *ca.* 1150°C for the contacted pigeonite-augite pair in both poikilitic and non-poikilitic areas. The pigeonite in the non-poikilitic area clearly has higher Ca and Fe composition than that in the poikilitic area, although the composition is scattered in both Ca and Fe compositions compared with that in the poikilitic area (Fig. 12). In many cases it ranges from  $\text{En}_{65}\text{Fs}_{28}\text{Wo}_7$  to  $\text{En}_{60}\text{Fs}_{27}\text{Wo}_{13}$  (Fig. 12). Minor element compositions further exhibit the difference of pyroxenes between the poikilitic and non-poikilitic areas.  $\text{TiO}_2$  of the low-Ca pyroxene in the poikilitic area increases from 0.05 wt% to 0.3 wt% (Fig. 13a).  $\text{Al}_2\text{O}_3$  also increases from 0.3 wt% to 1 wt%, and Al and Ti are positively correlated.  $\text{TiO}_2$  of the pigeonite in the non-

Table 1. Representative electron microprobe analyses (wt%) of major phases in Y-793605.

Poikilitic area						
	Low-Ca pyroxene (Ca, Fe-poor)	Low-Ca pyroxene (Ca, Fe-rich)	Augite	Olivine (Core)	Maskelynite (Core)	Maskelynite (Rim)
SiO <sub>2</sub>	56.0	54.7	52.0	38.6	55.5	59.8
Al <sub>2</sub> O <sub>3</sub>	0.3	0.8	1.9		27.9	25.5
TiO <sub>2</sub>	0.1	0.2	0.5		0.1	0.2
FeO	13.4	14.4	8.9	26.7	0.5	0.4
MnO	0.4	0.5	0.4	0.5		
MgO	28.0	23.6	16.7	33.7	0.2	0.1
CaO	1.4	5.6	17.6	0.2	10.9	8.2
Na <sub>2</sub> O			0.2		4.5	4.9
K <sub>2</sub> O					0.3	0.4
Cr <sub>2</sub> O <sub>3</sub>	0.4	0.5	0.8	0.1		
V <sub>2</sub> O <sub>3</sub>			0.1			
NiO			0.1			
P <sub>2</sub> O <sub>5</sub>	0.1	0.4	0.1		0.2	0.1
Total	100.1	100.7	99.3	99.8	100.1	99.6
<i>En</i>	76.6	66.2	48.7	69.2		
<i>Fs</i>	20.5	22.6	14.4	30.8		
<i>Wo</i>	2.8	11.2	36.9			
<i>An</i>					56.4	46.8
<i>Ab</i>					42.1	50.7
<i>Or</i>					1.5	2.5

Non-poikilitic area						
	Maskelynite (Core)	Maskelynite (Rim)	Olivine (Core)	Pigeonite (Ca, Fe-poor)	Pigeonite (Ca, Fe-rich)	Augite
SiO <sub>2</sub>	54.9	57.2	36.9	54.0	53.2	52.2
Al <sub>2</sub> O <sub>3</sub>	27.6	26.5		0.6	1.1	1.7
TiO <sub>2</sub>	0.1	0.2		0.7	0.6	0.8
FeO	0.5	0.4	29.5	17.0	14.9	10.0
MnO			0.6	0.8	0.5	0.4
MgO	0.2	0.1	32.5	22.9	21.3	16.4
CaO	11.1	9.7	0.2	3.7	7.1	17.1
Na <sub>2</sub> O	4.4	5.0		0.1	0.1	0.3
K <sub>2</sub> O	0.3	0.3				
Cr <sub>2</sub> O <sub>3</sub>		0.1		0.2	0.5	0.8
V <sub>2</sub> O <sub>3</sub>						0.1
NiO			0.1			
P <sub>2</sub> O <sub>5</sub>	0.2	0.1				0.2
Total	99.3	99.6	99.8	100.0	99.3	
<i>En</i>			66.3	65.2	61.3	47.8
<i>Fs</i>			33.7	27.2	24.0	16.4
<i>Wo</i>				7.6	14.7	35.8
<i>An</i>	56.9	50.6				
<i>Ab</i>	41.5	47.3				
<i>Or</i>	1.6	2.1				

\* Cation totals for maskelynites (O=24): core (poikilitic) 14.8, rim (poikilitic) 14.6, core (non-poikilitic) 14.8, rim (non-poikilitic) 14.8.

Table 2. Representative electron microprobe analyses (wt%) of minor phases in Y-793605.

Poikilitic and non-poikilitic areas						
	Chromite (Core)	Chromite (Rim)	Ilmenite	P-rich Phase	Olivine (Altered rim)	Impact melt vein
SiO <sub>2</sub>	0.2			4.7	50.5	44.1
Al <sub>2</sub> O <sub>3</sub>	5.0	5.9		1.6	0.1	4.9
TiO <sub>2</sub>	0.8	8.7	54.0	0.1	0.1	0.5
FeO	28.0	36.1	39.3	30.3	23.5	18.2
MnO	0.4	0.5	0.7	0.3	0.3	0.5
MgO	4.1	4.1	4.1	0.1	13.5	23.1
CaO		0.1		0.3	0.1	5.3
Na <sub>2</sub> O				0.1		1.0
K <sub>2</sub> O				0.1		0.1
Cr <sub>2</sub> O <sub>3</sub>	60.5	40.7	0.6	0.5	0.2	0.6
V <sub>2</sub> O <sub>3</sub>	0.6	0.5	0.4			0.2
NiO				0.1	0.1	
P <sub>2</sub> O <sub>5</sub>	0.1			22.3	0.5	0.7
Total	99.7	96.6	99.1	60.5	88.9	99.2
<i>En</i>						
<i>Fs</i>						
<i>Wo</i>						
Magmatic inclusion in olivine						
	Low-Ca pyroxene (Core)	High-Ca pyroxene (Core)	Si-rich glass (Si-poor)	Si-rich glass (Si-rich)		
SiO <sub>2</sub>	50.2	46.6	68.7	93.2		
Al <sub>2</sub> O <sub>3</sub>	7.0	9.6	19.0	4.3		
TiO <sub>2</sub>	0.6	2.9	0.6	0.4		
FeO	14.9	7.4	0.8	0.3		
MnO	0.6	0.4		0.1		
MgO	24.2	12.5	0.3			
CaO	1.3	19.1	1.7	1.3		
Na <sub>2</sub> O		0.3	1.6			
K <sub>2</sub> O			4.1			
Cr <sub>2</sub> O <sub>3</sub>	0.2	0.2				
V <sub>2</sub> O <sub>3</sub>	0.1	0.2	0.1			
NiO						
P <sub>2</sub> O <sub>5</sub>	0.1		0.5			
Total	99.2	99.2	97.4	99.6		
<i>En</i>	72.3	41.0				
<i>Fs</i>	25.0	13.7				
<i>Wo</i>	2.7	45.3				

poikilitic area has clearly higher concentration (0.4–0.9 wt%) than that in the poikilitic area. Al is also more enriched, and  $\text{Al}_2\text{O}_3$  ranges from 0.6 wt% to 1.3 wt%. However, unlike low-Ca pyroxenes in the poikilitic area, an Al-Ti diagram (Fig. 13a) shows two different trends for individual pigeonite grains in the non-poikilitic area. This trend is due to complex zoning in Ti of the pigeonite in the non-poikilitic area. The first trend is from high-Ti and medium-Al composition ( $\text{TiO}_2$ : 0.7 wt%;  $\text{Al}_2\text{O}_3$ : 0.6 wt%) to medium-Ti and medium-Al composition ( $\text{TiO}_2$ : 0.4 wt%;  $\text{Al}_2\text{O}_3$ : 0.6 wt%). In such pigeonite,  $\text{TiO}_2$  decreases from 0.7 wt% to 0.5 wt%, but then increases to 0.6 wt% from the core

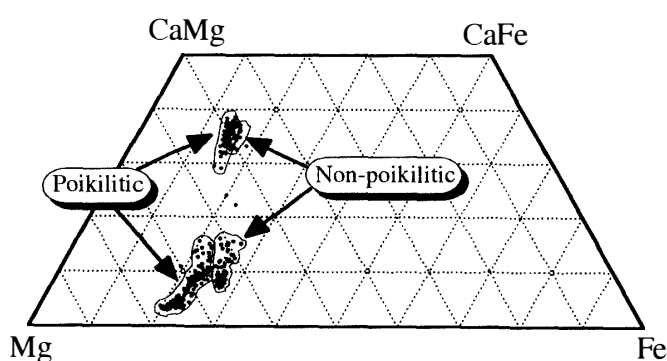


Fig. 12. Pyroxene quadrilateral showing pyroxene compositions of Y-793605,51-2. Pyroxenes in the non-poikilitic area have clearly more Fe-rich compositions than those in the poikilitic area. Note the coherent zoning trend of compositions toward the Ca-poor and Mg-rich contents. Mg: enstatite, Fe: ferrosilite, CaMg: diopside, and CaFe: hedenbergite.

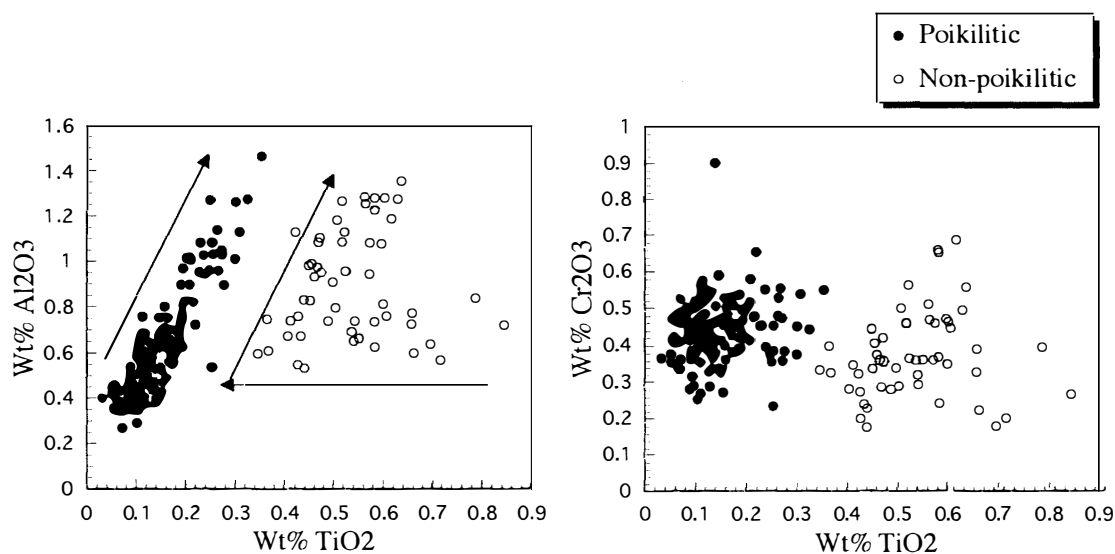


Fig. 13. a) Al vs Ti in low-Ca pyroxenes in Y-793605,51-2. The low-Ca pyroxenes in the poikilitic area show a continuous trend toward the Ti-Al-rich contents, while those in the non-poikilitic area are more Ti-rich and show two different trends. b) Cr vs Ti in low-Ca pyroxenes in Y-793605,51-2. Cr contents do not show a clear continuous trend, unlike Al.

to the rim, while Al monotonously increases toward the rim.  $\text{Cr}_2\text{O}_3$  in the low-Ca pyroxene oikocryst increases from 0.3 wt% to 0.5 wt% towards the rim (Fig. 13b). Cr zoning of the pigeonite in the non-poikilitic area does not show systematic change.

### 3.2.2. Olivine

Olivine is fairly uniform in major element composition in individual grains, but different grains show a weak compositional variation from  $\text{Fa}_{26}$  to  $\text{Fa}_{35}$ . Olivines in the non-poikilitic area is slightly more Fe-rich ( $\text{Fa}_{30-36}$ : Avg.  $\text{Fa}_{34}$ ) than those in the poikilitic area ( $\text{Fa}_{26-35}$ : Avg.  $\text{Fa}_{31}$ ) (Fig. 14). Olivines in the non-poikilitic area show a tight distribution, whereas those in the poikilitic area show a wider bell-shaped distribution. Minor elements in olivines do not show significant difference between the poikilitic and non-poikilitic area. CaO contents are nearly homogeneous or show slight decrease from the core (0.3 wt%) to the rim (0.1 wt%). Unlike other achondrites, olivine has up to 0.1 wt% NiO, indicating formation under oxidizing conditions. As stated before, olivine is extensively altered along the outer edge and the interior cracks (Fig. 4). Altered portion is enriched in Si, K and P, while poor in Fe and Mg. The total sum of these portions is generally low (83–89 wt%) presumably due to presence of unanalyzed elements like S.

### 3.2.3. Maskelynite

Maskelynite is weakly zoned in composition. No significant compositional difference can be observed from the maskelynites in both textures. The composition typically ranges from  $\text{An}_{58}\text{Ab}_{41}\text{Or}_1$  to  $\text{An}_{47}\text{Ab}_{50}\text{Or}_3$  (Fig. 15). However, the real composition is probably more albite-rich due to Na loss during microprobe analysis. Minor element zoning in maskelynites also does not show difference between the poikilitic and non-poikilitic textures (Fig. 16). K increases toward the rim ( $\text{K}_2\text{O}$ : 0.3–0.6 wt%). FeO decreases from the core to the rim (0.6–0.3 wt%), but then increases (0.3–0.4

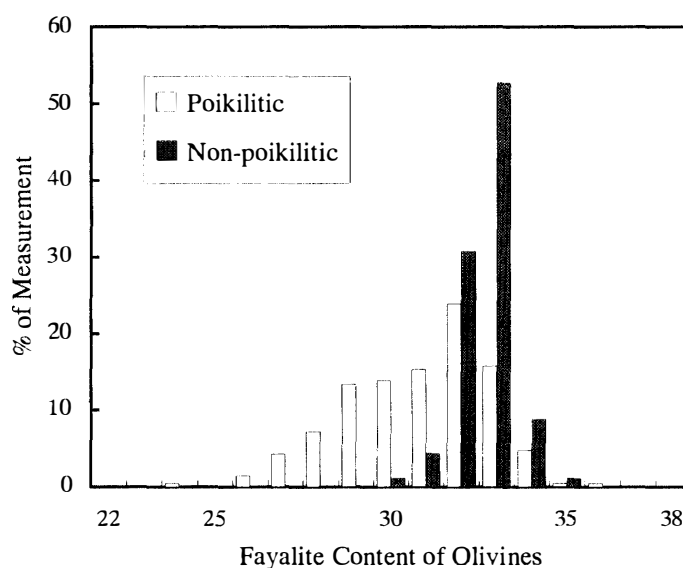


Fig. 14. Compositional distributions of olivines in Y-793605,51-2. Note that olivines in the non-poikilitic area are more Fe-rich and show narrower distributions than those in the poikilitic area. Data from 300 analyses of 105 individual grains.

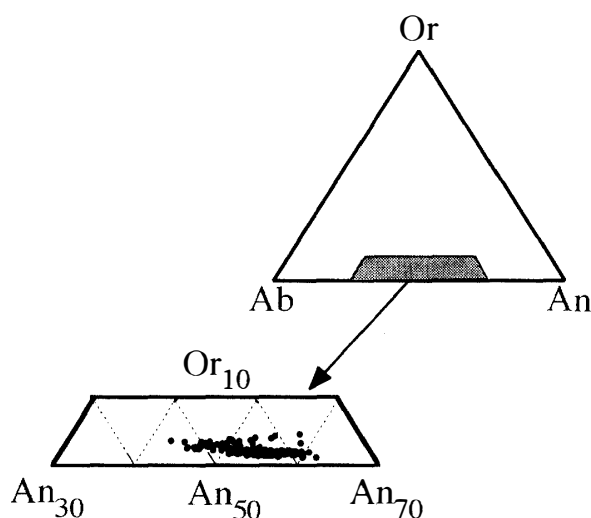


Fig. 15. Major element compositions (anorthite, albite, and orthoclase components) of maskelynites in Y-793605,51-2. No significant compositional difference was seen between poikilitic and non-poikilitic maskelynites.

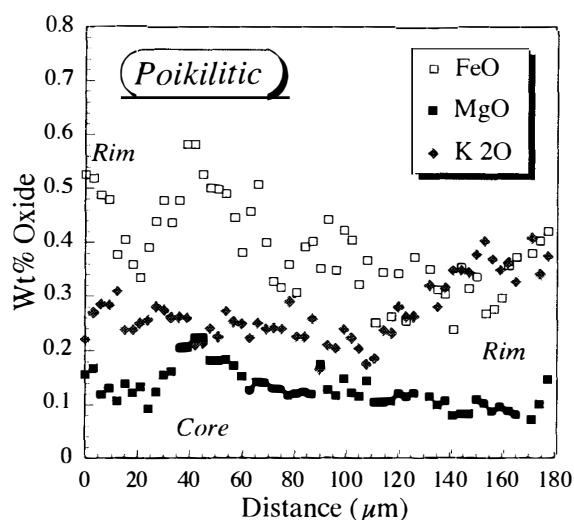


Fig. 16a. Fe, Mg, and K zoning profiles of Y-793605 maskelynites in the poikilitic area.

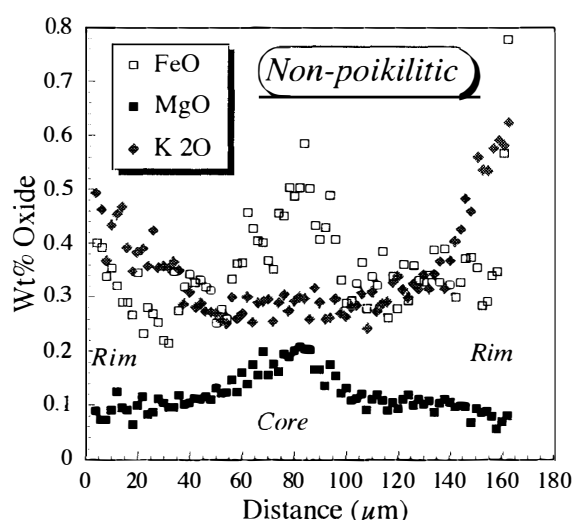


Fig. 16b. Same as Fig. 16a but for non-poikilitic area.

wt%). MgO decreases from 0.2 wt% to 0.1 wt% toward the rim.

#### 3.2.4. Chromite

Chromites are up to 200  $\mu\text{m}$  in size in both textures and they are euhedral. They also show chemical zoning toward the rim of ulvöspinel-rich component (Fig. 17). Chromites in the poikilitic area have 1 wt%  $\text{TiO}_2$ , 5.5 wt%  $\text{Al}_2\text{O}_3$ , 25 wt% FeO, 6 wt% MgO, and 60 wt%  $\text{Cr}_2\text{O}_3$  in the core. At the rim,  $\text{TiO}_2$  is 1.5 wt%,  $\text{Al}_2\text{O}_3$  is 7 wt%, FeO is 7 wt%, MgO is 6 wt%, and  $\text{Cr}_2\text{O}_3$  is 56 wt%. Chromites in the non-poikilitic area have similar compositions. The largest chromite shows a wider range of zoning than the others.  $\text{TiO}_2$  is 1–9 wt% and  $\text{Cr}_2\text{O}_3$  is 60–40 wt%. The equilibration temperature deduced from Fe-Mg partitioning between olivine and chromite included in olivine ( $K_D = (\text{Fe}/\text{Mg})^{\text{spinel}} / (\text{Fe}/\text{Mg})^{\text{olivine}}$ ) and Cr/(Cr+Al) ratio of chromite

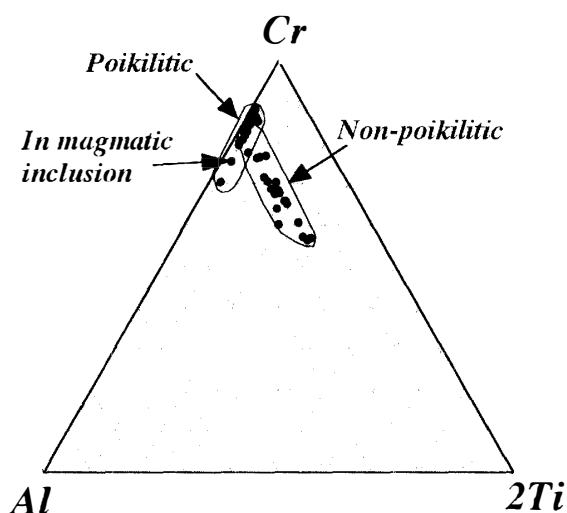


Fig. 17. Atomic ratios of Cr (chromite), Al (Al-spinel), and 2Ti (ulvöspinel) for chromites in Y-793605,51-2. Chromites in the non-poikilitic are zoned toward the Ti-rich (ulvöspinel) component.

suggests *ca.* 850–950°C (ENGI, 1983). However, it is not clear whether this temperature is really equilibration temperature, because both olivine and chromite are cumulus phase that might have no relation to each other.

### 3.2.5. Accessory phases

Ilmenite contains up to 5 wt% MgO and 1 wt% Cr<sub>2</sub>O<sub>3</sub>. In the non-poikilitic area, P-rich aggregates of very fine grains (<1 μm) are present (Fig. 11). Microprobe analyses also show enrichment of Fe, but the beam must be overlapped. The total sum is extremely low (60 wt%). Similar compositional phases are also observed as small isolated laths in the non-poikilitic area.

### 3.2.6. Magmatic inclusions

Magmatic inclusions in the olivines usually contain Si-rich feldspathic glass and Al-Ti-rich pyroxenes (Fig. 9). Si-rich glass observed in the inclusions can be separated into two groups. One group has about 60 wt% SiO<sub>2</sub>, and also contains 18 wt% Al<sub>2</sub>O<sub>3</sub>, 1.5 wt% CaO, 2 wt% Na<sub>2</sub>O and 4 wt% K<sub>2</sub>O. Another glass is rich in SiO<sub>2</sub> (SiO<sub>2</sub>: 93 wt%) and contains 4 wt% Al<sub>2</sub>O<sub>3</sub> and 1 wt% CaO. Na<sub>2</sub>O and K<sub>2</sub>O are less than 0.1 wt% in this glass. The presence of two different types of glass indicates liquid immiscibility as suggested by HARVEY *et al.* (1993). The pyroxene in the magmatic inclusion has high Al (Al<sub>2</sub>O<sub>3</sub>:~15 wt%) and Ti (TiO<sub>2</sub>:~3.5 wt%). The low and high Ca pyroxene pair in the magmatic inclusion (Fig. 18) suggests an equilibration temperature of *ca.* 950°C (LINDSLEY and ANDERSEN, 1983). However, this temperature is somewhat uncertain due to high Al and Ti contents, and several different compositional pyroxenes are present. Chromite is rarely observed in the inclusion, but it contains ~10 wt% Al<sub>2</sub>O<sub>3</sub>. Ilmenite has a nearly identical composition to that in the non-poikilitic area.

## 3.3. X-ray diffraction study of pyroxene

A single pyroxene crystal (~500 μm in size) was analyzed by the single crystal X-ray diffraction technique (precession camera) with Zr-filtered MoKα (λ=0.7107Å) radiation. The pyroxene grain was mounted on a glass fiber using oxybenzon. The (hk0)\* and (h0l)\* reciprocal nets were photographed by a precession camera with 0.1

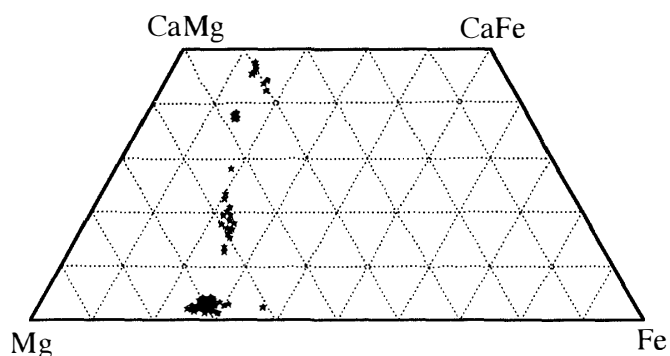


Fig. 18. Pyroxene quadrilateral showing pyroxene compositions in magmatic inclusions enclosed by Y-793605 olivines. Several kinds of pyroxenes are present. Some pyroxenes have extremely Wo-rich components. They are not plotted in this figure, because they are out of the quadrilateral. Mg: enstatite, Fe: ferrosilite, CaMg: diopside, and CaFe: hedenbergite.

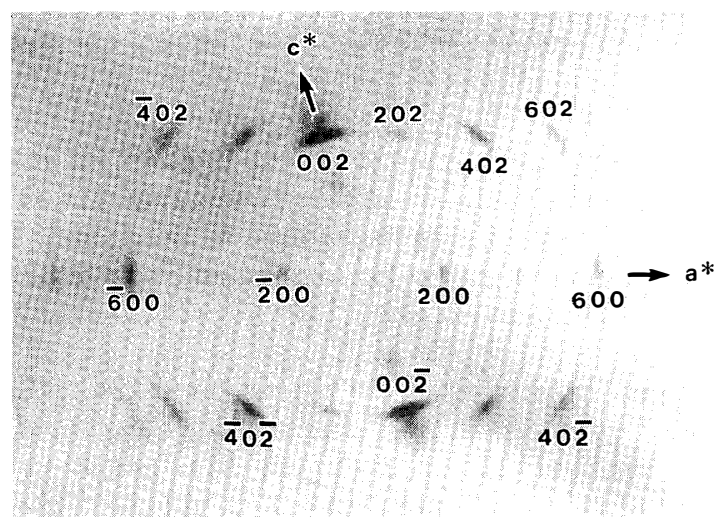


Fig. 19. X-ray diffraction photo of  $(h0l)^*$  plane by precession camera. Diffuse streaks of reflections are characteristic due to shock.

mm slit. Exposure times were 53–67 hours with 35 kV, 15 mA. The photos reveal streaked reflections showing intense shock effects (Fig. 19). This observation is consistent with the complete maskelynitization of the plagioclase, and the shock effect affected mineralogy on not only macroscopic scale (*e.g.*, faulted pyroxene twins) but the atomic scale. We infer that this crystal belongs to a monoclinic crystal system. The cell dimensions deduced from reflections on  $(hk0)^*$  and  $(h0l)^*$  planes give  $a$ :  $9.4 \pm 0.2 \text{ \AA}$ ,  $b$ :  $8.88 \pm 0.15 \text{ \AA}$ ,  $c$ :  $5.28 \pm 0.1 \text{ \AA}$ ,  $\beta = 108 \pm 0.5^\circ$ . Although these cell dimensions have large errors due to obscure image of reflections, they indicate that this pyroxene is augite. Microprobe analysis of this pyroxene also reveals that it is an augite of  $\text{En}_{53}\text{Fs}_{17}\text{Wo}_{30} \sim \text{En}_{52}\text{Fs}_{16}\text{Wo}_{32}$ , suggesting that it came from a poikilitic area. The large size of this augite also supports a poikilitic origin.

#### 4. Implications for Y-793605 Petrogenesis

It is obvious that Y-793605 is an igneous rock that contains abundant cumulus phases of Mg-rich olivine and chromites. As stated before, olivines and chromites in the non-poikilitic area have nearly identical compositions to those in the poikilitic area. This indicates that these phases in the non-poikilitic area are also cumulus. However, the olivine in the poikilitic area has a wider compositional distribution and is more Mg-rich than that in the non-poikilitic area. We infer that olivine in the non-poikilitic area experienced near-solidus or subsolidus re-equilibration after accumulation, because these olivines maintained contact with Fe-rich interstitial melt. In contrast, olivines surrounded by a pyroxene oikocryst had no chance to be highly re-equilibrated. Pigeonites in the non-poikilitic area clearly have more Fe-Ca-rich compositions than those in the poikilitic area (Fig. 12). The distinct chemical composition of pigeonite between the poikilitic and non-poikilitic area is also apparent for minor elements (Fig. 13). Continuous zoning of major elements in the large pigeonite oikocryst suggests a fractional crystallization in a closed system (Fig. 12). This is also seen from Al and Ti zoning in Fig. 13a. The volume of the system must be fairly large. The drop of Ti in the core of pigeonite from the non-poikilitic area (Fig. 13a) will reflect co-crystallization of ilmenite, whereas increase of Ti at the rim will be due to end of ilmenite precipitation or a larger effect of a small volume of the interstitial liquid. However, more complex history is possible. It seems that pigeonites in the non-poikilitic area formed from different compositional magma or by different igneous processes because there is little overlap of chemical composition of both major and minor elements between the poikilitic and non-poikilitic low-Ca pyroxene. Maskelynites in the non-poikilitic area have almost the same composition as those in the poikilitic area, and their zoning patterns of minor elements are quite similar (Fig. 16).

From mineralogy of major and minor phases in both poikilitic and non-poikilitic areas, the inferred crystallization sequence of minerals observed in Y-793605 is as follows: First, initial crystallization of cumulus phases (olivine and chromite) from the parent magma occurred. Then, low-Ca pyroxenes crystallized and then augite crystallized. The pyroxenes grew into large oikocrysts, poikilitically enclosing cumulus phases. Eventually, small interstitial melts were formed between the boundaries of oikocrysts and it became non-poikilitic areas. Plagioclase began to crystallize from the evolved melt along with pigeonite, and ongoing crystallization of pyroxenes caused that the pigeonite in the non-poikilitic area is more Ca-Fe-rich than the oikocrysts. Small amount of augite in the non-poikilitic area then formed. Finally, all phases especially in the non-poikilitic areas experienced re-equilibration. Olivine in the non-poikilitic area became more Fe-rich and showed a narrower compositional distribution. The faulted pyroxene twins and maskelynitization of plagioclase were due to impact after crystallization of Y-793605 whole rock. However, it is not clear whether Y-793605 was ejected from Mars by this impact.

### 5. Petrogenetic Relation to ALH77005 and LEW88516

It should be noted that Y-793605 shows strong affinities to previously known lherzolitic shergottites ALH77005 and LEW88516 in mineralogy and petrology (HARVEY *et al.*, 1993; TREIMAN *et al.*, 1994; IKEDA, 1994). From many lines of evidence, Y-793605 would follow a similar crystallization history to ALH77005 and LEW88516 whose formation model has been proposed by HARVEY *et al.* (1993). This model can generally apply to Y-793605 as stated before. From mineral chemistry of olivine, Y-793605 resembles LEW88516 rather than ALH77005. Fe-rich olivine of Y-793605 in the non-poikilitic area shows a closer relationship to LEW88516 than ALH77005, because LEW88516 olivines in the non-poikilitic area also have a wider compositional distribution ( $Fa_{30-40}$ ) and are more Fe-rich (avg.  $Fa_{35}$ ) than those in the poikilitic area (avg.  $Fa_{31}$ ) (HARVEY *et al.*, 1993; TREIMAN *et al.*, 1994). On the other hand, ALH77005 olivines do not show compositional difference between the poikilitic and non-poikilitic areas (HARVEY *et al.*, 1993; TREIMAN *et al.*, 1994). Low-Ca pyroxene compositions of Y-793605 in the poikilitic area are more Fe-rich than those of ALH77005, and nearly correspond to those of LEW88516 in Fig. 4 of HARVEY *et al.* (1993). However, Y-793605 does not contain Ca-Fe-rich low-Ca pyroxenes as shown in LEW88516 pyroxene plots in Fig. 4 of HARVEY *et al.* (1993) and Fig. 3 of TREIMAN *et al.* (1994). TREIMAN *et al.* (1994) shows a nearly identical compositional trend between ALH77005 and LEW88516 lowest-Ca pyroxenes. From these comparisons, it is difficult to indicate closer similarity of Y-793605 pyroxenes to ALH77005 or LEW88516 pyroxenes. Indeed, pyroxene equilibration temperature of Y-793605 in the poikilitic area is nearly identical to those of ALH77005 and LEW88516 pyroxenes (HARVEY *et al.*, 1993; ISHII, 1979), although these temperatures might bear some errors. Maskelynite compositions of Y-793605 are almost equal to those of ALH77005 and LEW88516.

As discussed above, many lines of evidence show similarity of Y-793605 to ALH77005 and LEW88516. However, it is difficult to conclude that Y-793605 is paired with ALH77005 or LEW88516 in the sense that Y-793605 originated in the same strewn field because Y-793605 is slightly distinct from them in mineral chemistry. The largest difference of Y-793605 mineralogy from both ALH77005 and LEW88516 is that Y-793605 does not contain Ca phosphates, although a local sample heterogeneity can not be ruled out. It will be very difficult that the meteorite found in Yamato Mountains are paired with those from Allan Hills and Lewis Cliff, because Yamato Mountains is more than 3000 km apart from Allan Hills and 2500 km from Lewis Cliff. However, it is possible that Y-793605 originated from the same igneous body in Mars as ALH77005 and LEW88516 did, and was excavated by the same shock event. From this point of view, all three meteorites could have originated from the same geological source in Mars. The difference of Y-793605 from ALH77005 and LEW88516 is quite minor, and HARVEY *et al.* (1993) and TREIMAN *et al.* (1994) discussed the same origin of ALH77005 and LEW88516 in Mars. Thus, it can be concluded that Y-793605 has originated from the same igneous body or rock as ALH77005 and LEW88516.

## 6. Conclusions

(1) Y-793605 is a new martian meteorite identified in the Japanese Antarctic meteorite collection, and it can be classified as a lherzolithic shergottite.

(2) Y-793605 is mainly constituted of a poikilitic texture, and partly contains a non-poikilitic area. A large pyroxene oikocryst encloses rounded olivine and euhedral chromite aggregates. The non-poikilitic areas are distinct from the poikilitic ones because they contain abundant maskelynite.

(3) Olivines are not zoned and generally Mg-rich ( $\text{Fa}_{26-35}$ ). Olivine in the non-poikilitic area is more Fe-rich and shows a narrower distribution than that in the poikilitic area. Pyroxenes in the non-poikilitic area are also more Fe-rich than those in the poikilitic area. Augites are usually present along the rim of the oikocryst in the poikilitic area. Equilibration temperature of pyroxene pairs indicates approximately 1150°C. Olivine sometimes contains trapped magmatic inclusions that are mainly composed of Si-rich glass and Al-Ti-rich pyroxenes.

(4) X-ray diffraction study of pyroxene shows intense shock, which is compatible with the presence of maskelynite, faulted pyroxene twins, and undulatory extinction of pyroxenes and olivine.

(5) The crystallization sequence of minerals in Y-793605 is considered to have begun by initial crystallization of olivine and chromite. Then, low-Ca pyroxenes poikilitically grew enclosing cumulus phases (olivine and chromite) with later augite, and became a large oikocryst. Eventually, small interstitial melts formed between the oikocryst boundaries, and plagioclase began to crystallize from the melt along with pigeonite. Minor augite then crystallized in the non-poikilitic area. Finally, all phases experienced re-equilibration.

(6) Y-793605 shows close affinities to previously known lherzolithic shergottites, ALH77005 and LEW88516. Olivine composition of Y-793605 is nearly identical to that of LEW88516, and very similar to that of ALH77005. Pyroxene and maskelynite compositions are almost the same among the three. However, Y-793605 does not contain Ca-phosphates, unlike ALH77005 and LEW88516. Although it is difficult to consider that Y-793605 is paired with ALH77005 or LEW88516 in the sense that Y-793605 arrived in the same fall with them, we infer that Y-793605 originated from the same igneous body or rock in Mars as ALH77005 and LEW88516.

## Acknowledgments

We thank Dr. H. KOJIMA of NIPR for the sample. We are indebted to Dr. T. ISHII, Mr. O. TACHIKAWA and Mr. H. YOSHIDA of University of Tokyo for technical assistance. Discussions with Prof. H. TAKEDA of Chiba Institute of Technology and Dr. G. A. MCKAY of NASA Johnson Space Center were very helpful. Constructive review by Drs. P. H. WARREN and A. TSUCHIYAMA improved the manuscript. This work was partially supported by Ito Science Foundation, JSPS (Japan Society for the Promotion of Science) Research Fellowships for Young Scientists, the Grant-in-Aid for Encouragement of Young Scientists by the Japanese Ministry of Education, Science and Culture (No. 08740410), and the Cooperative program (No. 12), 1996 provided by Ocean Research Institute, University of Tokyo.

### References

- ENGI, M. (1983): Equilibria involving Al-Cr spinel: Mg-Fe exchange with olivine. Experiments, thermodynamic analysis, and consequences for geothermometry. *Am. J. Sci.*, **283-A**, 29–71.
- HARVEY, R. P., WADHWA, M., MCSWEEN, H. Y., Jr. and CROZAZ, G. (1993): Petrography, mineral chemistry and petrogenesis of Antarctic shergottite LEW88516. *Geochim. Cosmochim. Acta*, **57**, 4769–4783.
- IKEDA, Y. (1994): Petrography and petrology of the ALH-77005 shergottite. *Proc. NIPR Symp. Antarct. Meteorites*, **7**, 9–29.
- ISHII, T., TAKEDA, H. and YANAI, K. (1979): Pyroxene geothermometry applied to a three-pyroxene achondrite from Allan Hills, Antarctica and ordinary chondrites. *Mineral. J.*, **9**, 460–481.
- LINDSLEY, D. H. and ANDERSEN, D. J. (1983): A two-pyroxene thermometer. *Proc. Lunar Planet. Sci. Conf.*, 13th, Pt. 2, A887–A906 (*J. Geophys. Res.*, **88**, Suppl.).
- MAYEDA, T. K., YANAI, K. and CLAYTON, R. N. (1995): Another martian meteorite. *Lunar and Planetary Science XXVI*. Houston, Lunar Planet. Inst., 917–918.
- MCKAY, D. S., GIBSON, E. K., Jr., THOMAS-KEPRTA, K. L., VALI, H., ROMANEK, C. S., CLEMETT, S. J., CHILLIER, X. D. F., MAECHLING, C. R. and ZARE, R. N. (1996): Search for past life on Mars: Possible relic biogenic activity in martian meteorite ALH84001. *Science*, **273**, 924–930.
- MCSWEEN, H. Y., Jr. (1985): SNC meteorites: Clues to martian petrologic evolution. *Rev. Geophys.*, **23**, 391–416.
- MCSWEEN, H. Y., Jr. (1994): What we have learned about Mars from SNC meteorites. *Meteoritics*, **29**, 757–779.
- MCSWEEN, H. Y., Jr., TAYLOR, L. A. and STOLPER, E. M. (1979a): Allan Hills 77005: A new meteorite type found in Antarctica. *Science*, **204**, 1201–1203.
- MCSWEEN, H. Y., Jr., STOLPER, E. M., TAYLOR, L. A., MUNTEAN, R. A., O'KELLEY, G. D., ELDRIDGE, J. S., BISWAS, S., NGO, H. T. and LIPSCHUTZ, M. E. (1979b): Petrogenetic relationship between Allan Hills 77005 and other achondrites. *Earth Planet. Sci. Lett.*, **45**, 275–284.
- MIKOUCHI, T. and MIYAMOTO, M. (1996a): A new member of Iherzolitic shergottite from Japanese Antarctic meteorite collection: Mineralogy and petrology of Yamato-793605. *Antarctic Meteorites XXI*. Tokyo, Natl Inst. Polar Res., 104–106.
- MIKOUCHI, T. and MIYAMOTO, M. (1996b): Comparative mineralogy of Antarctic Iherzolitic shergottites ALH 77005, LEW 88516 and Y 793605. *Meteorit. Planet. Sci.*, **31**, Suppl, A89–A90.
- TREIMAN, A. H. (1995): A petrographic history of martian meteorite ALH84001: Two shocks and an ancient age. *Meteoritics*, **30**, 294–303.
- TREIMAN, A. H., MCKAY, G. A., BOGARD, D. D., MITTFELDLT, D. W., WANG, M.-S., KELLER, L., LIPSCHUTZ, M. E., LINDSTROM, M. M. and GARRISON, D. (1994): Comparison of the LEW88516 and ALHA77005 martian meteorites: Similar but distinct. *Meteoritics*, **29**, 581–592.
- YANAI, K. (1995): Re-searching for martian rocks from diogenite-diogenitic achondrites. *Lunar and Planetary Science XXVI*. Houston, Lunar Planet. Inst., 1533–1534.

*(Received August 30, 1996; Revised manuscript accepted May 29, 1997)*